Interfacial Structure and Dynamics of Siloxane Systems: PDMS−Vapor and PDMS−Water

Ahmed E. Ismail,* Gary S. Grest, David R. Heine,† and Mark J. Stevens

Sandia National Laboratories, Albuquerque, New Mexico 87185

Mesfin Tsige

Department of Physics, Southern Illinois University, Mail Code 4401, Carbondale, Illinois 62901

Received December 17, 2008; Revised Manuscript Received February 20, 2009

ABSTRACT: Using a fully atomistic force field for polydimethylsiloxane developed by Smith et al. [*J. Phys. Chem. B* **2004**, *108*, 20340], we study the interfacial properties of polydimethylsiloxane (PDMS) as well as its interactions with water. We determine the surface tension of methyl- and hydroxyl-terminated PDMS chains with lengths between 20 and 100 repeat units and find good agreement between simulation results and experimental observations. The width of the polymer liquid−vapor interface is shown to depend on both molecular weight and temperature. The surface tension and contact angle are determined for the PDMS−water binary system using several different geometries and calculation methods. At 300 K, the surface tension of roughly 41 mN/m and contact angle of ≈108° for chains with 100 repeat units are in excellent agreement with experimental data. The width of the interface in both the PDMS and water layers increases with temperature, although the computed widths are significantly smaller than the liquid−vapor widths of the individual liquids. The diffusion constant measured for low concentrations of water molecules permeating through PDMS shows a wide degree of variation as a result of "caging" effects caused by local density inhomogeneities. At larger concentrations, aggregation of the water molecules leads to phase separation. Finally, the degrees of alignment of the methyl groups and siloxane backbones at the interface are found to decrease with temperature but are augmented in the presence of an interface with water.

I. Introduction

Siloxanes, and in particular poly(dimethylsiloxane) (PDMS), have a number of exceptional physical properties that make them desirable for a range of industrial applications. For instance, because of its high degree of backbone flexibility, PDMS has the lowest known glass transition temperature (150 K) of any polymer. In addition, because of its high degree of chemical stability, PDMS can also be used at relatively high temperatures. These properties make PDMS and its derivatives ideal for applications such as adhesives,[1] coatings,[2] and encapsulants.[3] In addition to its industrial versatility, PDMS has one of the simplest chemical structures of any non-hydrocarbon polymer, enabling studies of its properties based on its atomic structure and dynamics. Using molecular dynamics (MD) simulations, we investigate a number of interfacial properties of PDMS.

The properties of PDMS at its liquid−vapor interface have been studied experimentally. Fox et al.[4] present results for the surface tensions of very short PDMS chains up to 17 repeat units in length as well as very long chains, while Sauer and Dee[5,6] and Jalbert et al.[7] have studied the surface tension of PDMS melts as a function of chain length for intermediate-weight polymers. The latter results confirm the scaling law $\gamma \sim M_w^{-2/3}$ (where M_w is the molecular weight) proposed by Siow and Patterson for short polymer chains.[8]

Because one of the common applications of PDMS is as a sealant against water penetration, it is important to understand the interaction of PDMS with water. Diffusion of water through PDMS has been the subject of numerous experimental studies; these measurements typically involve permeation[9−11] or sorption[12] studies. Several attempts have also been made to determine the diffusion constant using molecular dynamics,[13,14] following the work of Sok et al.,[15] who studied the diffusion of helium and methane through siloxanes; however, these calculations have been performed for very small systems. The resulting estimates for the diffusion constant show variations of almost an order of magnitude for both experimental measurements and simulation results, indicating the difficulty associated with determining the transport of water through PDMS. The discrepancy is caused in part by "caging" effects, first observed in polymer melts by Takeuchi,[16] in which local variations in density through the melt can cause small molecules attempting to permeate through the melt to become trapped, limiting diffusion.[17−20]

The contact angle and surface tension are often used to characterize the bulk PDMS−water interface. Measurements of the advancing contact angle of the PDMS−water interface have been made by multiple investigators;[21−23] typical values show a hydrophobic interface, with contact angles between 98° and 112°. The surface tension of the interface has not received as much attention, although Fox et al. have obtained limited results using a drop-weight apparatus.[4]

There have been a number of recent studies of chain orientation in the vicinity of interfaces. Kim and co-workers[24] recently performed experimental measurements of PDMS monolayers at an air−water interface. Simulation studies include the work of Tsige et al.[25] and Smith et al.,[26] both of which examined PDMS interacting with a silica surface.

We have previously studied PDMS melts[27] using the united-atom class I potential of Sok et al.[15] and an explicit-atom class II potential developed by Sun and Rigby.[28,29] We have also examined the structure and relaxation of end-linked PDMS networks.[30] In the present paper, we examine the behavior of PDMS at the liquid−vapor interface, as well as its interactions with water, using a Buckingham (or exponential-6) force field for PDMS developed by Smith et al.[31] We examine properties such as the surface tension, contact angle, and interfacial width

* Corresponding author. E-mail: aismail@sandia.gov.
† Present address: Science and Technology Division, Corning, Inc., SP-TD-01-1, Corning, NY 14831.

10.1021/ma802805y CCC: $40.75
Published on Web 04/01/2009

Table 1. Mixing Terms for Nonbonded Lennard-Jones Interactions between SPC/E Water and PDMS Using the Smith et al.[31] Force Field

nonbonded pair[a]	ε_{ij} (kcal/mol)	σ_{ij} (Å)
Si−O$_W$	0.1948	3.490
O−O$_W$	0.1764	2.993
C−O$_W$	0.1147	3.292
H−O$_W$	0.0390	3.069

[a] No mixing terms were calculated for nonbonded interactions including hydrogen from SPC/E water molecules.

as a function of temperature, chain length, and end group. Our results are consistent with the available results in the literature.

We briefly review our simulation methodology, including the force field, techniques, and calculations employed, in the following section. We present and discuss our findings for pure PDMS in section III and for the PDMS−water interface in section IV before summarizing our conclusions in section V.

II. Methodology

A. Force-Field Description and Simulation Methodology. As discussed above, our previous simulations of PDMS[27] used both a united-atom force field[15] and a class II explicit-atom force field.[28,29] Structural calculations using the united-atom force field showed large deviations from experimental measurements. While the class II force field offered better agreement with experiment, the large number of "mixed geometry" terms in the force field led to unacceptably slow performance for very large systems. Also, in our previous work on the surface tension of alkanes,[32] we found that explicit-atom force fields agreed with experimental surface tension data more closely than united-atom force fields. Consequently, we model the PDMS molecules using the explicit-atom Buckingham force field developed by Smith et al.,[31] which contains terms describing the nonbonded, bond, angle, and torsional terms. For the water molecules, we use the SPC/E water model,[33] which was found to be the best available three-point model for interfacial calculations in a previous study of the water liquid−vapor surface tension.[34] To obtain the mixing terms needed to describe the interactions between the PDMS and water, it was necessary to fit the Buckingham potential to a Lennard-Jones potential for distances $r > r^*$, where $U_B(r^*) = 3k_BT$, before applying the standard arithmetic mixing rules for Lennard-Jones potentials. (The value of $3k_BT$ was chosen as the cutoff as it allows for a reasonable fit for the r^{-12} repulsion while avoiding the problems associated with the presence of the maximum in the Buckingham potential.) The Lennard-Jones cutoff, as well as the switching distance for the long-range electrostatic interactions, was set to 10 Å. Since the H−H Lennard-Jones well depth is set to zero for SPC/E water, no Lennard-Jones mixing terms were computed between the PDMS atoms and the hydrogen atoms in water. The resulting parameters for the mixing terms are shown in Table 1.

All simulations were performed using the LAMMPS simulation package.[35] The equations of motion were integrated by the Verlet method using a 1 fs time step. For both the *NVT* and *NPT* ensemble calculations, the temperature is maintained using a Nosé-Hoover thermostat with a 100 fs damping constant. In addition, the *NPT* ensemble calculations employed a Nosé-Hoover barostat with a 500 fs damping constant to control the pressure.

B. Interfacial Properties of PDMS. To determine the surface tension of PDMS chains, a bulk melt was allowed to equilibrate at 300 K for at least 2 ns. The melt contained 500 chains of $N_p = 20$ monomer units, 200 chains of $N_p = 50$ monomer units, or 100 chains of $N_p = 100$ monomer units; for a given simulation, the terminal groups were either all methyls or all hydroxyls. The initial box dimensions were approximately $L_x = L_y = 125$ Å, with the z-direction chosen to match experimental density. Equilibration of the liquid phase followed the method used by Sides et al.,[27] in which randomly oriented chains were placed in a box, with overlaps removed by the use of a soft potential, followed by a 4 ns run in the *NVT* ensemble. Following the initial equilibration period, the periodic boundary condition in the z-direction was removed, and for each chain which crosses the boundary, duplicate configurations of the chain were created; the chain whose center of mass remains within the original simulation box was kept. The z-dimension was then increased to $L_z = 165$ Å for the $N_p = 20$ system and $L_z = 188$ Å for the $N_p = 50$ and $N_p = 100$ melts, ensuring that the periodic images of the resulting slab do not interact with one another.

For a pure liquid in equilibrium with its vapor, the surface tension γ_P can be determined from pressure calculations:[36,37]

$$\gamma_P = \frac{L_z}{2}\left(\langle p_z\rangle - \frac{1}{2}\langle p_x + p_y\rangle\right) \quad (1)$$

However, truncating the Lennard-Jones potential causes an underestimation of the surface tension by neglecting the long-range contributions. A better estimate for the surface tension can be obtained by including a "tail correction", which is computed from the density profile $\rho(z)$:[38]

$$\gamma_{tail} = \frac{\pi}{2}\int_{-\infty}^{\infty}\int_{-1}^{1}\int_{r_c}^{\infty} r^3\frac{dU(r)}{dr}g(r)(1 - 3s^2)\times (\rho(z)\rho(z - sr) - (\rho_G(z))^2)\, dr\, ds\, dz \quad (2)$$

where $U(r)$ is a pairwise potential, $g(r)$ is the radial distribution function, $\rho(z)$ is the observed interfacial profile, $s = \cos\theta$ in cylindrical polar coordinates, and $\rho_G(z)$ is a Gibbs dividing surface:

$$\rho_G(z) = \rho_c + \frac{\Delta\rho}{2}\,\mathrm{sgn}(z) \quad (3)$$

where $\rho_c = (\rho_l + \rho_v)/2$ and $\Delta\rho = \rho_l - \rho_v$ are the average density and the difference in density between the liquid and vapor phases, respectively. It is assumed in using eq 2 that the radial distribution function $g(r) \approx 1$ for $r \geq r_c$, while, on the basis of our previous work,[32,34,39,40] we fit the density profile $\rho(z)$ to an error function. For the purposes of this calculation, the profile is shifted such that the interface is located at $z = 0$.

In the case of the Buckingham potential, only the r^{-6} dispersion term is necessary to evaluate eq 2 since the exponential terms are negligible for $r \geq r_c$. For a species like PDMS with multiple pairwise potentials, the tail correction γ_{tail} becomes a sum over all pairwise potentials. The overall surface tension γ is determined as the sum of the direct simulation result and the tail correction: $\gamma = \gamma_P + \gamma_{tail}$. For sufficiently large cutoffs, it can be shown that the results of an explicit Ewald summation for both the Lennard-Jones and electrostatic interactions yields the same results as the sum of the simulation with a cutoff plus the tail correction given in eq 2.[40]

C. Diffusion of Water in PDMS Melts. To measure the diffusion of water through a PDMS melt, 1, 5, 20, or 120 SPC/E water molecules (corresponding to concentrations of 0.012, 0.060, 0.25, and 1.45 wt %) were inserted into a pre-equilibrated bulk PDMS melts containing either 100 20-mers or 20 100-mers of either methyl-terminated or hydroxyl-terminated chains. A short *NVT* simulation using a soft potential was performed to remove any overlaps between the embedded water molecules and the bulk PDMS. Following this, a short simulation (0.5 ns) in the *NPT* ensemble was used to establish the system at $p =$ 1 atm for $T = 300$ and 400 K. The dynamics of the resulting configuration was then measured using a molecular dynamics

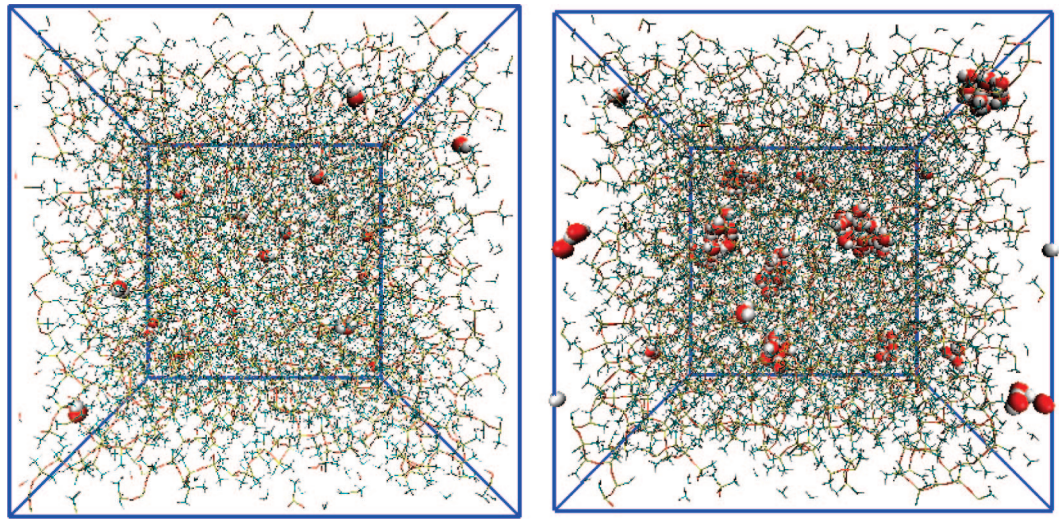

Figure 1. (left) Diffusion of 20 water molecules (0.25 wt % water) through a methyl-terminated PDMS melt of chain length 100 after 2 ns of simulation. (right) Onset of phase segregation for a system containing 120 water molecules in a melt of methyl-terminated PDMS chains (N_p = 100; 1.45 wt % water) after 2 ns of simulation. PDMS molecules are shown in bond representation; atoms in water molecules are represented by van der Waals spheres.

simulation in the *NVT* ensemble. The positions of the oxygen atoms in the water molecules were recorded every 250 fs over the course of a simulation covering 10 ns or longer for the systems at 0.012 and 0.060 wt % and 7 ns or longer for the systems at 0.25 and 1.45 wt %. A sample configuration showing the positions of the water molecules for the 0.25 and 1.45 wt % systems is shown in Figure 1. The trajectory information was used to generate a plot of mean-square displacement of the oxygen atoms as a function of time. Determining the normal diffusion regime, the diffusion coefficient was then computed from the Einstein equation:

$$D = \lim_{\Delta t \to \infty} \frac{(r(t + \Delta t) - r(t))^2}{6\Delta t} \tag{4}$$

where the ensemble average is taken over both the trajectory of all the water oxygen atoms and all available initial starting configurations.

D. Surface Tension and Contact Angle of PDMS−Water Interfaces. In addition to determining the diffusion properties of water in PDMS, we also studied the behavior of the PDMS−water interface. Three different water geometries were examined: a hemispherical drop with radius 60 Å, a spherical drop with radius 50 Å, and a slab with thickness 50 Å. The two drop geometries were used to test if initial drop shape had any effect on the measured contact angle, while the slab geometry permitted an additional route for calculation of interfacial properties. In each simulation, an initial downward velocity $v_z = -0.1$ Å/ps was applied to the drop, ensuring that it will come into contact with the surface. After the two surfaces come into contact, the water and PDMS surfaces were allowed to reach equilibrium. Following equilibration, the simulations were run for an additional 2 ns using an *NVT* ensemble at 300 K.

For the drop simulations, the positions of the water molecules were recorded every 10 ps; the contact angle was then calculated using the isochoric density-binning method of Werder et al.[41] Given the contact angle, one can then determine the surface tension of the PDMS−water interface via Young's equation:[42]

$$\gamma_{PW} = \gamma_P - \gamma_W \cos\theta \tag{5}$$

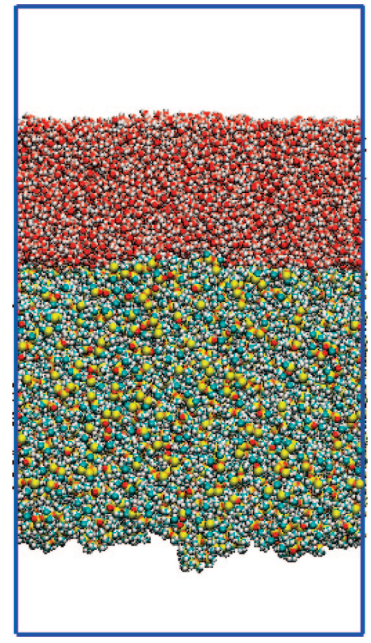

Figure 2. Equilibrated configuration of a water slab in contact with a methyl-terminated PDMS slab of chains with length N_p = 100 at 300 K. Silicons are shown in yellow, oxygens in red, carbons in light blue, and hydrogens in gray.

where γ_P and γ_W are the surface tensions of PDMS and SPC/E water as determined by simulation, θ is the PDMS−water contact angle, and γ_{PW} is the surface tension of the PDMS−water interface. For the slab−slab interface, as shown in Figure 2, the difference between the pressures normal and parallel to the interface is equal to the sum of the surface tensions for the liquid−vapor interfaces for water and PDMS plus the surface tension of the liquid−liquid interface:

$$\gamma_{sim} = \gamma_W + \gamma_{PW} + \gamma_P = L_z\left(\langle p_z\rangle - \frac{1}{2}\langle p_x + p_y\rangle\right) \tag{6}$$

Because of the low vapor pressures of both water and PDMS at 300 K, there were essentially no molecules in either vapor, and periodic boundary conditions can be used in the z-direction without significantly altering the results obtained from eq 6.

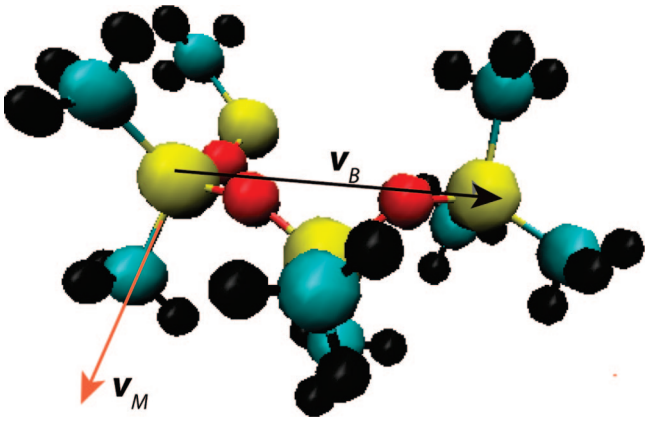

Figure 3. Orientation vectors $\mathbf{v}_M$ and $\mathbf{v}_B$ used to compute the methyl and backbone order parameters S_M and S_B. Silicons are shown in yellow, oxygens in red, carbons in light blue, and hydrogens in black.

No tail corrections of the form given in eq 3 have been used in obtaining the surface tension of the PDMS−water interface.

E. Molecular Orientation near the PDMS−Water Interface. In addition to the surface tension, we also examined the orientation of methyl groups near the PDMS−water interface. We follow in this work the prior studies of Pierce et al.,[43] who examined semifluorinated alkanes, and Tsige and Grest,[44] who studied perfluorinated alkanes at the liquid−vapor interface. For these simulations, the slab−slab geometry shown in Figure 2 was examined. We can characterize the effect of the interface on methyl group orientation as a function of position using the orientation order parameter S:

$$S(z) = \frac{1}{2}\langle 3\cos^2\theta - 1\rangle \tag{7}$$

where θ is the angle between a vector that represents the molecular orientation and the unit vector z normal to the interface. Here $\langle\cdots\rangle$ represents an ensemble average over all vectors within a specified slab in the z-direction. The value of S is zero if the vectors are randomly oriented, 1 if all vectors are aligned normal to the interface, and −0.5 if all vectors are aligned parallel to the interface. To characterize molecular orientation of the methyl groups S_M, we define the orientation vector $\mathbf{v}_M$ for the methyl groups as the segment connecting the C of the methyl group to the point corresponding to the center of the three hydrogen atoms. We also characterize the backbone orientation S_B, defining as an orientation vector $\mathbf{v}_B$ to be the relative positions of two silicon atoms separated by two oxygen atoms along the backbone of the chain. According to the definition of the order parameter, positive values of S_M and S_B indicate that the CH_3 groups and backbone prefer to align normal to the interface; negative values indicate a parallel alignment. We expect S_M and S_B to be negatively correlated, so that parallel alignment of the backbones leads to normal alignment of the methyl groups, and vice versa. Sample orientation vectors $\mathbf{v}_M$ and $\mathbf{v}_B$ are shown in Figure 3.

Knowing the orientations of the CH_3 groups and the backbone of a PDMS molecule should supplement our understanding of the orientation of the molecule near the interface. The other advantage of calculating and reporting these two orientations is that they can be observed experimentally using infrared−visible sum frequency spectroscopy techniques.[45]

III. PDMS Interfacial Properties

A. Surface Tension of PDMS. The surface tension of PDMS as a function of chain length and end group at 300 K is shown in Table 2. The surface tension of the methyl-terminated PDMS increases as a function of chain length, in agreement with the experimental results of Dee and Sauer,[5,6] although the numerical values determined by simulation are about 10% higher than those obtained from experiment. However, the work of Jalbert et al.[7] suggests that the surface tension of both methyl- and hydroxyl-terminated PDMS should decrease with increasing molecular weight. Although the present work does not support this finding, we do find, as did Jalbert et al., that the change in surface tension as a function of molecular weight is smaller for the hydroxyl-terminated PDMS than for the methyl-terminated PDMS. The surface tension of PDMS is very similar to that of alkane chains of comparable length,[32] which suggests that the methyl groups on the siloxane backbone play a larger role in determining the interfacial behavior than does the backbone itself.

Table 2. Surface Tension of PDMS at 300 K as a Function of Chain Length and Type

		surface tension,[a] mN/m		
N_p	chain type	γ_P	γ_{tail}	$\gamma = \gamma_P + \gamma_{tail}$
20	$-CH_3$	15.0	5.5	20.5
50	$-CH_3$	18.0	5.4	23.4
100	$-CH_3$	18.5	5.4	23.9
∞	$-CH_3$			26.0
20	−OH	16.4	5.2	21.6
50	−OH	17.3	5.0	22.3
100	−OH	18.0	4.7	22.7
∞	−OH			23.2
expt (ref 6)				21.0

[a] Uncertainty in γ_P and γ is less than 1.0 mN/m.

Using the $M_w^{-2/3}$ power law proposed by Siow and Patterson for low-weight polymers,[8] we can also determine upper bounds for the surface tension in the limit of an infinite-weight polymer. The infinite-weight limits for the methyl- and hydroxyl-terminated chains are also given in Table 2; the variation between the results for the $N_p = 100$ system and the infinite-length polymer is less than 10% for both methyl- and hydroxyl-terminated chains. The estimates for γ_∞ represent upper bounds, since it is expected that, at high molecular weights, the molecular weight dependence of the surface tension should be M_w^{-1} instead of $M_w^{-2/3}$.[5,46]

Examining the simulation and tail correction components to the surface tension, we find that the magnitude of the tail correction contribution γ_{tail} ranges between 20% and 25% of the overall surface tension γ. Overall, this is a much greater relative contribution to the surface tension than the long-range correction in water, which accounts for ∼10% of the overall surface tension at $T = 300$ K and a cutoff $r_c = 10$ Å.[34] This discrepancy is caused by the relative importance of electrostatic interactions in water compared to PDMS, as only the oxygens in SPC/E water have assigned LJ interactions, while all of the polymer atoms have LJ interactions.

The effect of temperature on surface tension was also examined; simulation results for temperatures between 300 and 450 K for methyl-terminated chains with lengths 20 and 100 are shown in Figure 4. The surface tension for both lengths decreases with temperature, as expected; however, the surface tension decreases more quickly for the $N_p = 100$ chains than for the $N_p = 20$ chains. In addition, the long-range contributions γ_{tail} to the surface tension decrease with temperature, both on an absolute scale and in its relative contribution to γ.

B. Intrinsic Width of PDMS Interface. The total interfacial width Δ and intrinsic interfacial width Δ_0 are related through the surface tension γ according to[47−51]

$$\Delta^2 = \Delta_0^2 + \frac{k_B T}{2\pi\gamma}\ln\left(\frac{L}{B_0}\right) \tag{8}$$

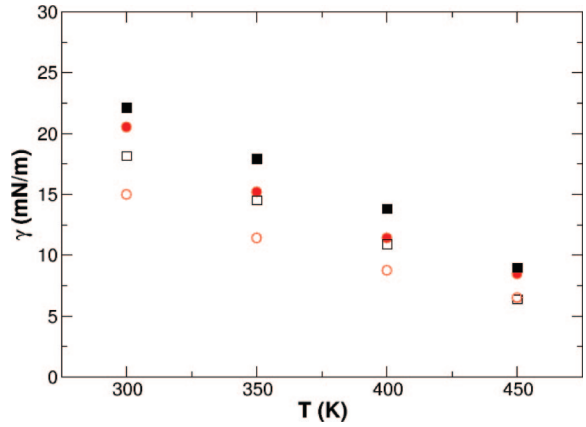

Figure 4. Surface tension of methyl-terminated PDMS as a function of temperature. Simulation results for γ_P (open symbols) and γ (filled symbols) are shown for chain lengths $N_p = 20$ (circles) and $N_p = 100$ (squares).

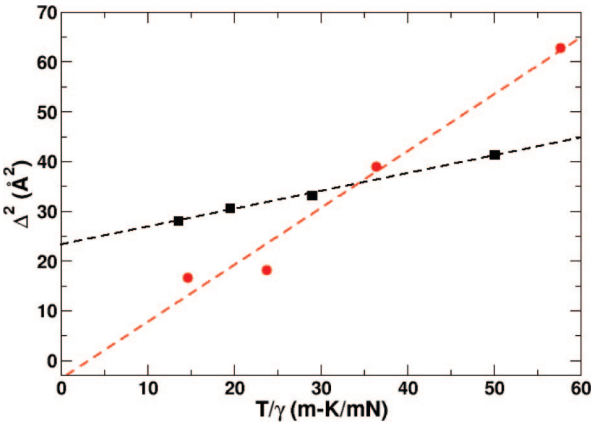

Figure 5. Interfacial width Δ^2 of $-CH_3$-terminated PDMS chains as a function of temperature divided by surface tension (T/γ) for chain lengths $N_p = 100$ (squares) and $N_p = 20$ (circles); regression lines represent the least-squares fit to eq 8.

where L is the length of the simulation box parallel to the interface and B_0 is an intrinsic parameter of the simulation. Sides et al.[39] and Ismail et al.[34] have previously shown for molecular systems that the density profiles used to determine the capillary width are best fit to error functions instead of to hyperbolic tangent functions. In our previous work on liquid−vapor interfaces of water,[34] we used the logarithmic dependence of Δ on the interfacial length L to derive an estimate for the surface tension γ. However, from eq 8, one can also determine the intrinsic width Δ_0 of the interface from knowledge of the total interfacial width Δ and of the surface tension $\gamma(T)$ as a function of temperature, while keeping the interfacial length L constant.[52]

Thus, using eq 8 to fit the temperature data given in Figure 5, we find that the intrinsic width of the methyl-terminated PDMS is $\Delta_0 = 4.8$ Å for $N_p = 100$. A significant chain length dependence exists: for $N_p = 20$, the intrinsic width is essentially zero, since $\Delta_0^2 \approx 0$. These values are substantially smaller than most estimates found for the intrinsic width of high-molecular-weight polymers,[53] reflecting a strong finite chain-length effect. This result is also consistent with the work of Mitrinović et al.,[54] who found that the interfacial width exhibited a strong molecular-weight dependence.

IV. PDMS−Water Interfacial Properties

A. Diffusion of Water in PDMS Melts. Computing the diffusion constant for a small permeant through a polymer melt can be challenging because it is possible for the permeant to become trapped within a region of the melt for significant periods of time.[17] The permeant consequently moves through the melt in a series of "hops"; in between these hops, it becomes stuck in a "cage", during which very little net displacement occurs. Our simulations demonstrate that the initial position of the water molecule in the melt can have a strong effect on the overall net displacement, suggesting that even relatively small inhomogeneities in the melt structure can have a large effect on diffusion.

As an example, we show in Figure 6 the position of the central oxygen atom of a single water molecule diffusing through a melt of methyl-terminated PDMS with $N_p = 100$ for three different starting positions within the melt. While two of the trajectories show that the water molecule travels through a substantial portion of the melt within 2 ns, one of the molecules is clearly caged within a single region for the entire length of the simulation. The averaged mean-square displacements for these three trajectories are also shown in Figure 7; the high-displacement particle would have a diffusion constant 10 times larger than the medium-displacement particle; a similar difference exists between the medium- and low-displacement particles. Figure 7 also demonstrates that the caged water molecule undergoes anomalous diffusion,[55] while the other particles are closer to the Einstein diffusion regime.

Results for the diffusion constant of water through PDMS at 300 and 400 K as a function of chain type and water concentration are shown in Table 3. As can be seen, at 300 K, diffusion rates slow down as a function of concentration for all four combinations of chain length and terminal group, particularly at higher concentrations. Such behavior is to be expected, as higher concentrations lead to greater aggregation of water molecules, which will diffuse through the polymer more slowly than individual molecules. Estimating the uncertainty in the measured diffusion constants is complicated by the presence of caging effects, which introduces systematic errors that are much larger than the statistical error inherent in determining the slope of the best-fit line; a sample of the mean square displacements versus time used to determine the diffusion constants D is shown in Figure 8.

The aggregation limit does not appear to have been reached at 400 K, as the diffusion constants for 0.01 and 0.06 wt % are comparable. Comparing the trajectories of the water molecules in Figure 6, we find that at 400 K the water molecules are significantly more mobile than the comparable molecules at 300 K. This is in part due to the lower density of PDMS at 400 K, which creates greater "holes" and decreases the probability of water molecules getting trapped in a given section of the polymer matrix.

There is a wide discrepancy in the values reported in the literature for the diffusion constant of water in PDMS. For instance, using MD simulations, Tamai et al.[13] obtain a diffusion constant $D = 1.5 \times 10^{-5}$ cm^2/s for a single SPC/E water molecule at 300 K moving through PDMS modeled using a united-atom GROMOS force field.[15] Fritz and Hoffman[14] report diffusion constants at 300 K ranging between 8×10^{-6} and 3.7×10^{-5} cm^2/s, although they used the pcff force field[56] to model PDMS instead of GROMOS. Some of the discrepancy between the studies may be the result of finite size effects; Tamai et al.[13] use only five chains of 30 repeat units per simulation, for a concentration of 0.16 wt %, while Fritz and Hoffman studied the motion of three water molecules in a single polymer with 220 repeat units (a concentration of 0.33 wt %). These concentrations appear to be at or above the solubility limit of water in PDMS, which has been estimated in various experiments to be between 0.1 and 0.2 wt % at 300 K.[10,57] The simulations of Tamai et al.,[13] which also examined diffusion for a water concentration of nearly 1 wt %, shows strong

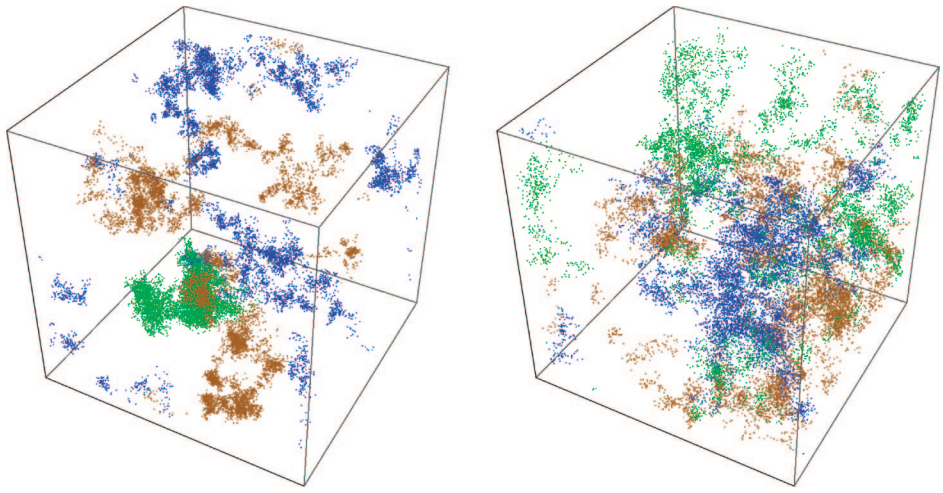

Figure 6. Trajectories for three water molecules placed at different initial positions within a melt of methyl-terminated PDMS chains of length 100 over a 2 ns interval at 300 K (left) and 400 K (right). At 300 K, two of the trajectories (blue and brown) exhibit "hopping," while a third (green) exhibits caging.

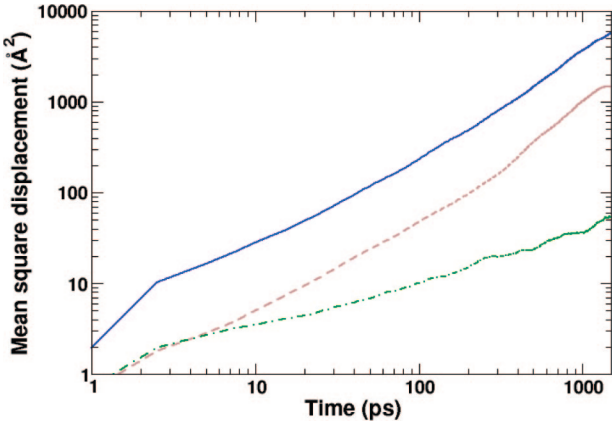

Figure 7. A log−log plot of mean-square displacement as a function of time for the three trajectories (blue solid line, brown dashed line, and green dash-dotted line) shown in the 300 K plot in Figure 6.

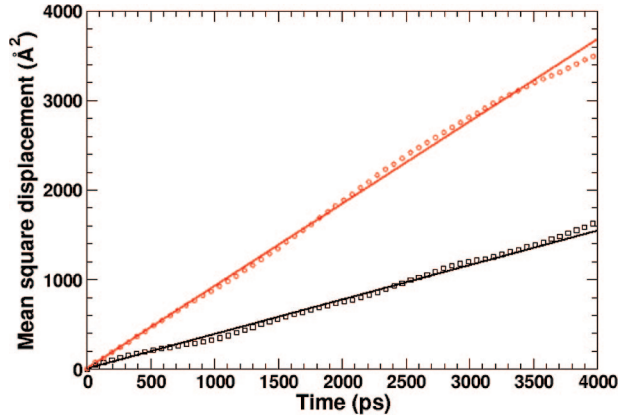

Figure 8. Plot of mean-square displacement vs time for the diffusion of water at 300 K through PDMS at a concentration of 0.060 wt % through a melt of chains of length 20 with methyl (black squares) and hydroxyl (red circles) terminal groups. Fit lines for determining the diffusion constant are also shown.

Table 3. Diffusion Constant of Water as a Function of Water Concentration and PDMS Chain Length and Type at $T = 300$ K and $p = 1$ atm

		diffusion constant, D ($\times 10^{-5}$ cm^2 s^{-1})				
		300 K			400 K	
N_p	chain type	0.012 wt %	0.06 wt %	0.25 wt %	0.012 wt %	0.06 wt %
20	−CH_3	2.15	0.62	0.56	7.87	9.05
20	−OH	1.91	1.58	0.63	15.0	7.42
100	−CH_3	2.50	1.04	0.78	6.80	9.54
100	−OH	3.19	0.90	0.81	8.79	7.44

evidence of phase segregation, as do our simulations (see Figure 1) for the highest water concentration studied.

Experimental results also show an equally wide divergence. The equilibrium sorption and permeation studies of Barrie and Machin[12] obtain a value of $D = 4 \times 10^{-5}$ cm^2/s, while the permeation studies of Okamoto et al.[9] lead to an estimate of $D = 1.45 \times 10^{-5}$ cm^2/s. Among more recent measurements, Favre et al.[10] obtain a diffusion constant of $D \approx 10^{-4}$ cm^2/s, while Watson and Baron[11] found the diffusion constant to be $D = 2 \times 10^{-5}$ cm^2/s. All experimental data have been reported at 300 K.

Comparing the results of our simulations to the previously reported studies, we find that our results are consistent with previous studies. For higher concentrations, aggregation effects can be significant in determining the transport coefficients for water in PDMS. Barrie and Platt found that clustering of water molecules into dimers and trimers can lead to a 3−5-fold reduction in the measured diffusion constants;[58] this result is consistent with our findings for the 0.06 and 0.25 wt % cases, in which dimer and trimer clusters are observed. As can be seen from Figure 1, as the concentration of water molecules increases, the water molecules are found almost exclusively in clusters. For the highest concentration studied, 1.25 wt %, we cannot exclude the possibility that, at long times, the water molecules will phase separate into a single cluster. This is consistent with the observed experimental miscibility of 0.1−0.2 wt % water in PDMS.[10,57]

B. Surface Tension and Contact Angle of PDMS−Water Interfaces. For the drop simulations near the interface, we note that only a short time is required for the drops to reach their final equilibrium shape. The initially spherical drop has obtained a slightly spheroidal shape by the time it contacts the surface, as shown in Figure 9. Within 50 ps, the initially spherical drop has become further oblate, and after 100 ps, there is very little change in the shape of the drop. Similar results were obtained for the initially hemispherical drop. Although only 100 ps was required for the final geometry to be obtained, the system was allowed to equilibrate for 1 ns to eliminate any transient effects

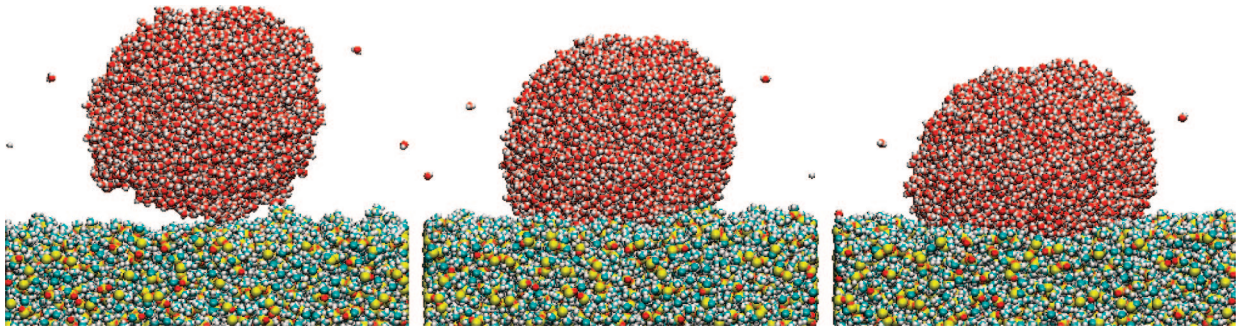

Figure 9. Evolution of the spherical water drop placed on top of a PDMS interface. Configurations shown at contact (left) and at 50 ps (center) and 100 ps (right) after contact.

Table 4. Surface Tension and Width Δ_P and Δ_W of PDMS−Water Interface for Methyl-Terminated Chains ($N_p = 100$) as a Function of Temperature for Interfacial Area $A = 15\,400$ Å^2

	surface tension,[a] mN/m				interfacial width,[b] Å			
temp (K)	γ_{sim}	γ_P	γ_W	γ_{PW}	Δ_P	Δ_W	$\Delta_{P,lv}$	$\Delta_{W,lv}$
300	127	23.9	61.8	41	3.3	2.8	5.3	3.1
350	109	17.5	47.0	45	3.8	3.0	5.5	3.8
400	95	14.0	37.6	44	4.2	3.3	5.8	4.6
450	79	10.0	30.6	39	4.8	3.5	6.4	5.7

[a] Uncertainties in PDMS surface tension measurements are less than 1.0 mN/m; uncertainties in water surface tension measurements are less than 3.0 mN/m. [b] Interfacial width $\Delta_{P,lv}$ for PDMS at its liquid−vapor interface are from the present work; interfacial width for water at its liquid−vapor interface taken from ref 34.

before collecting measurements for the surface tension and contact angle.

The drop simulations gave consistent results for both the spherical and hemispherical geometries. In each case, the contact angle was measured to be 108 ± 3°, in good agreement with experimental observations, which estimate the contact angle to be between 98° and 112°.[21−23] Our measurements for the contact angle show no dependence on the PDMS chain length, suggesting that there are not enough chain ends available at the surface to have a significant effect on the contact angle and that there would not be a substantial difference were hydroxyl groups substituted for the terminal methyl groups. Increasing the cutoff for the Lennard-Jones interaction to 16 Å likewise had no discernible effect on the contact angle of the drop.

For the slab−slab interface, which had water placed above a PDMS melt with $N_p = 100$, the right-hand side of eq 6 is equal to 127 mN/m. Given the values $\gamma_P = 24$ mN/m calculated above and $\gamma_W = 61.8$ mN/m calculated for SPC/E water,[34,40] we find that the interfacial surface tension is $\gamma_{PW} = 41$ mN/m. Comparing this to the value calculated for the drop geometries using eq 5 with the values of γ_P given above along with $\theta = 108°$, we obtain an estimate of $\gamma_{PW} = 39$ mN/m. These results, obtained by two different methodologies, are internally consistent as well as in excellent agreement with the experimental surface tension of 40 mN/m.[4] It is also possible to determine the variation of both the surface tension and the interfacial thickness as a function of temperature; these results are presented in Table 4. The surface tension of the PDMS−water interface shows little variation as a function of temperature.

C. Interfacial Width of PDMS−Water Interfaces. In addition to measuring the PDMS liquid−vapor interfacial width, it is also possible to measure the interfacial width in each liquid at the PDMS−water interface. The interfacial widths Δ_P and Δ_W are a function of the surface area; for the simulations performed here, the interfacial area is a constant, and therefore the widths of the different interfaces can be directly compared. As shown in Table 4, the intrinsic interfacial widths exhibit the

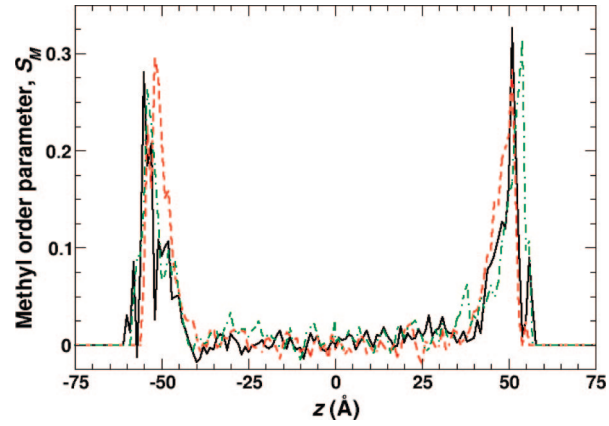

Figure 10. Methyl order parameter S_M as a function of position for chain lengths $N_p = 20$ (black solid curve), $N_p = 50$ (red dashed curve), and $N_p = 100$ (green dashed-dotted curve) of methyl-terminated PDMS at the liquid−vapor interface.

expected increase in temperature; however, the widths of both the PDMS and water layers at a PDMS−water interface are significantly smaller than the interfacial widths of PDMS and water at their respective liquid−vapor interfaces. This suggests that the presence of the neighboring liquid phase acts to suppress the intrinsic width of the interface.

D. Orientation near the PDMS−Water Interface. The orientations of the methyl groups on the PDMS chains are shown as a function of position in Figure 10 for the liquid−vapor interface. The order parameter S at the PDMS liquid−vapor interface shows similar behavior to that observed in fluoroalkanes,[44] varying from nearly 0 within the bulk and increasing to ∼0.3 near the liquid−vapor interface. There is little difference in the order parameter as a function of chain length, as the number of terminal groups is small compared to the total number of methyl groups for the three lengths (N_p = 20-, 50-, and 100-mers) studied. In addition, the difference between the order parameter profiles for methyl- and hydroxyl-terminated PDMS chains is negligible for the same reason.

Examining the profile of the backbone order parameter S_B for the binary PDMS−water system, shown in Figure 11, we see that there is a sharpening in the order parameter profile at the PDMS−water interface relative to the PDMS liquid−vapor interface. For the PDMS−water interface, the value goes from essentially zero to its maximum value near the interface within a 10 Å region; in the PDMS liquid−vapor system, this same change occurs over a 20 Å region. In addition to the sharpening of the interface, there appears to be greater alignment of PDMS chains in the presence of water. This is confirmed by plotting the orientational order parameter for the methyl groups, as defined by eq 7 and shown in Figure 12 for different PDMS−water systems as a function of temperature. For each

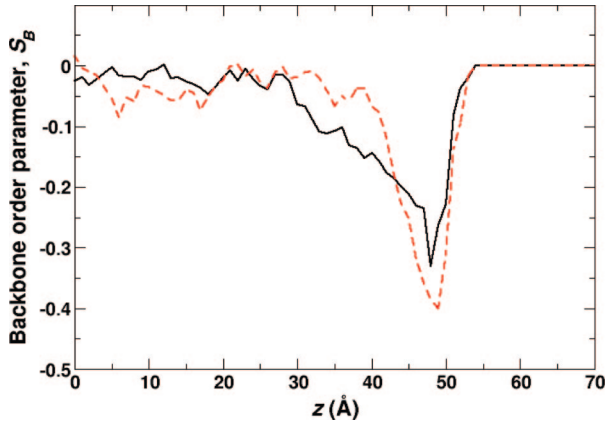

Figure 11. Backbone order parameter S_B for the Si backbone orientation as a function of position for PDMS chains of length 100 at the liquid−vapor interface (black solid curve) and at the PDMS−water interface (red dashed curve). The interface is located at approximately $z = 50$ Å.

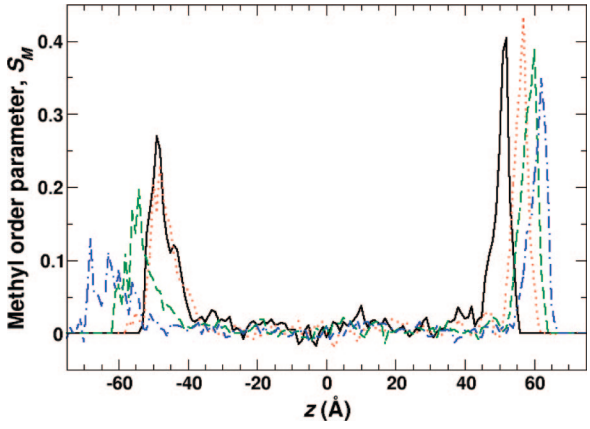

Figure 12. Methyl order parameter S_M as a function of position for chains of length 100 near the PDMS−water interface at 300 K (black solid curve), 350 K (red dotted curve), 400 K (green dashed curve), and 450 (blue dashed-dotted curve). The PDMS liquid−vapor interface is located between $z = -65$ Å and $z = -50$ Å; the PDMS−water interface is located at approximately $z = 50$ Å.

system, the PDMS liquid−vapor interface to the left shows a much weaker tendency toward alignment than does the PDMS−water interface on the right. While the alignment near the PDMS liquid−vapor interface becomes weaker as temperature increases, the variation with temperature at the PDMS−water interface is much smaller. This is consistent with the physical behavior of the system, as the PDMS liquid−vapor interface becomes less well-ordered as temperature increases. With water as an adjoining phase, the persisting orientation of chains parallel to the interface even as temperature increases may stem from the electrostatic interactions between the PDMS chains and the water.

However, there appears to be little evidence of significant amounts of hydrogen bonding between the water molecules and the oxygens on the PDMS chains. Following Lommerse et al.,[59] a hydrogen bond is defined here as a distance between a water hydrogen and a PDMS oxygen of less than 3 Å and a "bond angle" $\theta_{OHO} > 150°$. Even for PDMS chains protruding into the water layer, the concentration of hydrogen bonds is less than 0.1 per PDMS oxygen atom and drops rapidly as a function of distance away from the interface. We also find that chains lie more or less flat on the surface, with only minimal protrusions of individual chains normal to the interface. These results partially support the findings of Kim et al.,[24] who also found that chains lie parallel to the interface but also found that at high concentrations the oxygens along the backbone were exposed to the adjacent water phase, with the silicon atoms closer to the other PDMS chains. The low concentration of hydrogen bonds found in the present work suggests that a different arrangement of the backbone atoms may exist. That an alternate arrangement does occur is strongly supported by the fact that the water drops placed on top of a PDMS slab retained a droplike shape, indicating the hydrophobicity of PDMS. Coupled with the low surface tension of PDMS relative to that of water, these results explain why PDMS acts as a sealant.

V. Conclusions

Extensive molecular dynamics simulations based on the Smith et al. atomistic force field[31] have been performed to determine the interfacial and diffusion properties of PDMS. The results obtained for PDMS interfacial properties are in good agreement with results reported from both experimental and simulation studies of PDMS. Given our previous work, which found that united-atom force fields do not agree well with interfacial data for short polymer chains[32] and offer poor agreement with bulk properties for PDMS,[27] the present work indicates that explicit-atom models of PDMS are probably required for accurate measurements of interfacial properties. Examining PDMS liquid−vapor interfacial properties, we find that the Smith et al. potential slightly overestimates the PDMS liquid−vapor surface tension compared to the experimentally measured surface tension. The surface tension shows a strong dependence on chain length, as does the interfacial width.

Using the simulation-measured surface tensions of PDMS and SPC/E water, excellent agreement with experiment is obtained for the surface tension of the PDMS−water interface as well as the contact angle. This agreement persists across multiple geometries and multiple calculation methodologies. Diffusion constants for low concentrations of water molecules show reasonable agreement with experimental results. Aggregation of water molecules has been observed at higher concentrations, on the order of 1% by mass. Diffusion constants are observed to show significant variation as a function of initial location, and the observed trajectories consist of hops between "caged" configurations. Orientation effects are measured using backbone and methyl group order parameters. Strong alignment effects are observed near both the PDMS−vapor and PDMS−water interfaces. The magnitudes of the backbone and methyl order parameters are shown to depend significantly both on temperature and on whether the adjoining phase is PDMS vapor or liquid water.

Acknowledgment. Sandia is a multiprogram laboratory operated by Sandia Corporation, a Lockheed Martin Company, for the United States Department of Energy under Contract DE-AC04-94AL85000.

Note Added After ASAP Publication. This article posted ASAP on April 1, 2009. Equation 5 has been revised. The correct version posted on April 3, 2009.

References and Notes

(1) Benkoski, J. J.; Kramer, E. J.; Yim, H.; Kent, M. S.; Hall, J. *Langmuir* **2004**, *20*, 3246–3258.
(2) Abdellah, L.; Boutevin, B.; Youssef, B. *Prog. Org. Coat.* **1994**, *23*, 201–236.
(3) McDonald, J. C.; Whitesides, G. M. *Acc. Chem. Res.* **2002**, *35*, 491–499.
(4) Fox, H. W.; Taylor, P. W.; Zisman, W. A. *Ind. Eng. Chem.* **1947**, *39*, 1401–1409.
(5) Sauer, B. B.; Dee, G. T. *Macromolecules* **1991**, *24*, 2124–2126.
(6) Dee, G. T.; Sauer, B. B. *Macromolecules* **1993**, *26*, 2771–2778.
(7) Jalbert, C.; Koberstein, J. T.; Yulgor, I.; Gallagher, P.; Krukonis, V. *Macromolecules* **1993**, *26*, 3069–3074.

(8) Siow, K. S.; Patterson, D. *Macromolecules* **1971**, *4*, 26–30.
(9) Okamoto, K.; Nishioka, S.; Tsuru, S.; Sasaki, S.; K., T.; Kita, H. *Kobunshi Ronbunshu* **1988**, *45*, 993–999.
(10) Favre, E.; Schaetzel, P.; Nguyen, Q. T.; Clément, R.; Néel, J. *J. Membr. Sci.* **1994**, *92*, 169–184.
(11) Watson, J. M.; Baron, M. G. *J. Membr. Sci.* **1996**, *110*, 47–57.
(12) Barrie, J. A.; Machin, D. *J. Macromol. Sci., Phys.* **1969**, *3*, 645–672.
(13) Tamai, Y.; Tanaka, H.; Koichiro, N. *Macromolecules* **1994**, *27*, 4498–4508.
(14) Fritz, L.; Hofmann, D. *Polymer* **1997**, *38*, 1035–1045.
(15) Sok, R. M.; Berendsen, H. J. C.; Van Gunsteren, W. F. *J. Chem. Phys.* **1992**, *96*, 4699.
(16) Takeuchi, H. *J. Chem. Phys.* **1990**, *93*, 2062.
(17) Müller-Plathe, F. *J. Chem. Phys.* **1991**, *94*, 3192.
(18) Gray-Weale, A. A.; Henchman, R. H.; Gilbert, R. G.; Greenfield, M. L.; Theodorou, D. N. *Macromolecules* **1997**, *30*, 7296–7306.
(19) Greenfield, M. L.; Theodorou, D. N. *Mol. Simul.* **1997**, *19*, 329–361.
(20) Greenfield, M. L.; Theodorou, D. N. *Macromolecules* **2001**, *34*, 8541–8553.
(21) Rolland, J. P.; Van Dam, R. M.; Schorzman, D. A.; Quake, S. R.; DeSimone, J. M. *J. Am. Chem. Soc.* **2004**, *126*, 2322–2323.
(22) Lawton, R. A.; Price, C. R.; Runge, A. F.; Doherty, W. J., III.; Saavedra, S. S. *Colloids Surf., A* **2005**, *253*, 213–215.
(23) Bodas, D.; Khan-Malek, C. *Microelectron. Eng.* **2006**, *83*, 1277–1279.
(24) Kim, C.; Gurau, M. C.; Cremer, P. S.; Yu, H. *Langmuir* **2008**, *24*, 10155–10160.
(25) Tsige, M.; Soddemann, T.; Rempe, S. B.; Grest, G. S.; Kress, J. D.; Robbins, M. O.; Sides, S. W.; Stevens, M. J.; Webb, E. *J. Chem. Phys.* **2003**, *118*, 5132–42.
(26) Smith, J. S.; Borodin, O.; Smith, G. D.; Kober, E. M. *J. Polym. Sci., Part B: Polym. Phys.* **2007**, *45*, 1599–1615.
(27) Sides, S. W.; Curro, J. G.; Grest, G. S.; Stevens, M. J.; Soddemann, T.; Habenschuss, A.; Londono, J. D. *Macromolecules* **2002**, *35*, 6455.
(28) Sun, H.; Rigby, D. *Spectrochim. Acta A* **1997**, *53*, 1301–1323.
(29) Sun, H. *J. Phys. Chem. B* **1998**, *102*, 7338–7364.
(30) Heine, D. R.; Grest, G. S.; Lorenz, C. D.; Tsige, M.; Stevens, M. J. *Macromolecules* **2004**, *37*, 3857–3864.
(31) Smith, J. S.; Borodin, O.; Smith, G. D. *J. Phys. Chem. B* **2004**, *108*, 20340–20350.
(32) Ismail, A. E.; Tsige, M.; in 't Veld, P. J.; Grest, G. S. *Mol. Phys.* **2007**, *105*, 3155.
(33) Berendsen, H. J. C.; Grigera, J. R.; Straatsma, T. P. *J. Phys. Chem.* **1987**, *91*, 6269–6271.
(34) Ismail, A. E.; Grest, G. S.; Stevens, M. J. *J. Chem. Phys.* **2006**, *125*, 014702.
(35) Plimpton, S. J. *J. Comput. Phys.* **1995**, *117*, 1–9.
(36) Tolman, R. C. *J. Chem. Phys.* **1948**, *16*, 758–774.
(37) Kirkwood, J. G.; Buff, F. P. *J. Chem. Phys.* **1949**, *17*, 338.
(38) Blokhuis, E. M.; Bedeaux, D.; Holcomb, C. D.; Zollweg, J. A. *Mol. Phys.* **1995**, *85*, 665–669.
(39) Sides, S. W.; Grest, G. S.; Lacasse, M.-D. *Phys. Rev. E* **1999**, *60*, 6708–6713.
(40) in 't Veld, P. J.; Ismail, A. E.; Grest, G. S. *J. Chem. Phys.* **2007**, *127*, 144711.
(41) Werder, T.; Walther, J. H.; Jaffe, R. L.; Halicioglu, T.; Koumoutsakos, P. *J. Phys. Chem. B* **2003**, *107*, 1345–1352.
(42) Israelachvili, J. N. *Intermolecular and Surface Forces*; Academic Press: New York, 1992.
(43) Pierce, F.; Tsige, M.; Perahia, D.; Grest, G. S. *J. Phys. Chem. B* **2008**, *112*, 16012.
(44) Tsige, M.; Grest, G. S. *J. Phys. Chem. C* **2008**, *112*, 5029–5035.
(45) Yurdumakan, B.; Harp, G. P.; Tsige, M.; Dhinojwala, A. *Langmuir* **2005**, *21*, 10316–10319.
(46) Dee, G. T.; Sauer, B. B. *Adv. Phys.* **1998**, *47*, 161–205.
(47) Buff, F. P.; Lovett, R. A.; Stillinger, F. H. *Phys. Rev. Lett.* **1965**, *15*, 621–623.
(48) Huang, J. S.; Webb, W. W. *J. Chem. Phys.* **1969**, *50*, 3677–3693.
(49) Beysens, D.; Robert, M. *J. Chem. Phys.* **1987**, *87*, 3056–3061.
(50) Semenov, A. N. *Macromolecules* **1994**, *27*, 2732–2735.
(51) Lacasse, M.-D.; Grest, G. S.; Levine, A. J. *Phys. Rev. Lett.* **1998**, *80*, 309–312.
(52) Pierce, F.; Tsige, M.; Borodin, O.; Perahia, D.; Grest, G. S. *J. Chem. Phys.* **2008**, *128*, 214903.
(53) Shull, K. R.; Mayes, A. M.; Russell, T. P. *Macromolecules* **1993**, *26*, 3829–3836.
(54) Mitrinović, D. M.; Tikhonov, M.; Aleksey; Li, M.; Huang, Z.; Schlossman, M. L. *Phys. Rev. Lett.* **2000**, *85*, 582–585.
(55) Gusev, A. A.; Arizzi, S.; Suter, U. W. *J. Chem. Phys.* **1993**, *99*, 2221.
(56) Sun, H.; Mumby, S. J.; Maple, J. R.; Hagler, A. T. *J. Am. Chem. Soc.* **1994**, *116*, 2978.
(57) Rezac, M. E.; John, T.; Pfromm, P. H. *J. Appl. Polym. Sci.* **1997**, *65*, 1983.
(58) Barrie, J. A.; Platt, B. *Polymer* **1963**, *4*, 303–313.
(59) Lommerse, J. P. M.; Price, S. L.; Taylor, R. *J. Comput. Chem.* **1997**, *18*, 757–774.

MA802805Y